J. Fluid Mech. (1979), *vol.* 94, *part* 3, *pp.* 409–431
Printed in Great Britain

Measurements of turbulence in a zero-mean-shear mixed layer

By TREVOR J. McDOUGALL

Department of Applied Mathematics and Theoretical Physics,
University of Cambridge†

(Received 8 September 1978)

This paper is concerned with laboratory measurements of turbulence in a mixed layer and through a density interface, in the absence of a mean flow. The present results confirm the conclusion of Hopfinger & Toly (1976) that the turbulence in a mixed layer is not significantly affected by the slow entrainment of fluid across the bounding density interface. In a homogeneous fluid the turbulence intensity is found to be surprisingly non-uniform, even two grid mesh distances away from the grid. Velocity measurements have also been taken through a density interface (at the entraining boundary of a mixed layer) and the turbulence here varies in a manner that bears some resemblance to the theory of Hunt & Graham (1978). These velocity measurements were taken with a laser-Doppler anemometer and they were made possible by a novel experimental technique which eliminates the refractive index variations which normally occur in a turbulent, density-stratified liquid flow.

1. Introduction and review of the literature

Well-mixed layers of constant density often occur near boundaries in stratified fluids. The oceanic (or atmospheric) mixed layer is almost always capped by a shallow layer of high static stability. This interfacial region is called the diurnal or seasonal thermocline in the ocean, and in the atmosphere it is called the atmospheric inversion layer. This layer of high stability is turbulent only intermittently and it provides a virtual barrier to the transport of mass and heat (and other scalar properties, for example moisture or salinity). Momentum and energy can however be lost from the mixed layer by internal gravity waves which can propagate through the region of stable stratification beyond the mixed layer. A knowledge of the processes which cause entrainment across these density interfaces is imperative to be able to predict for example the depth of the mixed layer and the sea-surface temperature of the ocean.

Kraus & Turner (1967) were the first to model a mixed layer with surface inputs of both mechanical energy and buoyancy. This was also simulated in a laboratory experiment by Turner & Kraus (1967). The predictions of the theoretical model, and the results of the experiments for both the mixed layer depth and the temperature, showed good agreement with oceanic measurements over the course of a year. Since 1967 mixed layer models have attracted a great deal of attention and we do not intend to review the literature on this subject in detail. Excellent reviews have been given by Turner (1973), Niiler & Kraus (1977) and Gill & Turner (1976).

† Present address: Research School of Earth Sciences, The Australian National University, P.O. Box 4, Canberra 2600, ACT.

0022–1120/79/4257–7190 $02.00

The results of laboratory experiments on entrainment into the mixed layer caused by mechanical mixing have played an important role in guiding the choices of parameterization of entrainment which are used in numerical mixed layer models. These laboratory experiments can be divided into two categories: (i) those which are driven by a surface stress of some kind, and therefore exhibit a mean shearing flow, and (ii) those which are driven by oscillating grids of bars and so have no mean flow. The experiments with no mean flow are reviewed in detail below.

1.1. *Experiments with zero mean shear*

The first accurate measurements of entrainment into a mixed layer with zero mean shear were made by Turner (1968). He performed two types of experiment; the first type with only one layer stirred and the second type with both layers stirred. His results were presented in terms of overall parameters but have since been expressed in terms of the length and velocity scales of the turbulence near the density interface (see Turner 1973) by using the measurements of Thompson (1969). These measurements were made in a homogeneous fluid but they are the relevant scaling parameters at the base of the mixed layer (see §4 below). Turner showed that the entrainment of fluid into a mixed layer is independent of whether the other layer is stirred or not. This is because the mixing events are rare and can be considered statistically independent. The main result of Turner's experiments was that the entrainment velocity can be expressed as

$$u_e/u_1 \propto Ri^{-n} \quad \text{for} \quad Ri \gtrsim 7, \tag{1}$$

where Ri ($= g\Delta\rho l/\rho_0 u_1^2$) is the Richardson number based on the density difference $\Delta\rho$ between the layers and the integral length scale l and root-mean-square horizontal velocity u_1 of the turbulence near the interface. ρ_0 is a reference density. From his data, Turner quoted values of n in (1) of 1 when heat was the stratifying agent and $\frac{3}{2}$ when common salt was used. For $Ri \lesssim 7$, u_e/u_1 was the same for both salt and heat.

Thompson & Turner (1975) measured the properties of the turbulent velocity field as a function of distance from the vertically oscillated grid. The measurements were made by a hot film probe which rapidly rotated one revolution at a time to obtain a horizontally averaged measurement. They also investigated the flow produced by a single oscillating cylinder or square bar and found the character of the flow to depend on exactly what type of bar was used and at what stroke it was oscillated. Their measurements showed that for a grid of square bars which was oscillated at a stroke equal to the width of the bars, the root-mean-square horizontal velocity u_1 at a fixed distance from the grid was proportional to the frequency of oscillation of the grid f. The integral length scale l was found to be proportional to the distance z from the grid, i.e. $l = \beta z$ with $\beta = 0{\cdot}10$. The only formula which Thompson & Turner quote for the dependence of u_1 on z is their equation (13) [$u_1 \propto z^{-1{\cdot}5}$] which the authors point out is only an approximate expression, describing the results of *all* types of grid to within $\pm 50\,\%$. A better fit to their data for square bars (their figure 6*a*; see also figure 5.3 of Thompson 1969) is given by $u_1 \propto z^{-1}$. This has been pointed out by Hopfinger & Toly (1976) and it is unfortunate that the $z^{-1{\cdot}5}$ dependence has been so widely quoted.

Crapper & Linden (1974) have shown that the different powers n in (1) for heat and salt are due to the different Péclet numbers in the two sets of experiments ($Pe = u_1 l/\kappa$, where κ is the diffusivity of the stratifying agent). When the stratification

was caused by heat in Turner's experiments, the Péclet number was low (< 200) and molecular diffusion influenced the structure of the interface. For these low Péclet numbers there is a diffusive core in the centre of the interface across which all the transport of heat occurs by molecular diffusion. When the stratification is due to salt, the Péclet number is high ($\gg 200$) and the entrainment is controlled by non-diffusive processes. Crapper & Linden found that the interface thickness (non-dimensionalized by the integral length scale) was independent of the Richardson number and was also independent of Péclet number Pe when this was large (> 200). For small Pe they found that the interface thickness increased as Pe decreased.

Wolanski & Brush (1975) have provided confirmation that the ratio of the interface thickness to the turbulence length scale is independent of the Richardson number. They also found that the entrainment ratio u_e/u_1 was proportional to Ri^{-n} but found values of n as high as 3·7 when the stratification was produced by a suspension of clay particles, although their data are quite scattered. This result may have been influenced by non-Newtonian effects near the oscillating grids.

Long (1975, 1977) has asserted that the process by which the turbulence entrains fluid across an interface is the same for the experiments without mean shear as for those with mean shear. Kato & Phillips (1969), in a now classical experiment on entrainment into a mean shearing flow, found

$$u_e/u_* \propto Ri_*^{-1}, \tag{2}$$

where the velocity scale u_* (which is also used in the Richardson number) is the friction velocity based on the stress which is applied at the top of the mixed layer. In order to reconcile this -1 power law with the $-1{\cdot}5$ power law of Turner (1968) for salt, Long proposed that

$$\frac{u_1}{fS} \propto (g\Delta\rho D/\rho_0 f^2 S^2)^{-\frac{1}{6}}, \tag{3}$$

which implies that the turbulent velocity scale u_1 near the density interface is dependent on an overall Richardson number. One of the main aims of the present paper has been to investigate the influence of an interfacial density step on the velocity field in the mixed layer, and in particular to test the validity of (3). Hopfinger & Toly (1976) have measured the velocity field in a mixed layer with a continuously rotating hot film probe.† For fixed $\Delta\rho$ and l, (3) reduces to $u_1 \propto f^{\frac{3}{4}}$ (instead of $u_1 \propto f$) and Hopfinger and Toly have plotted u_1 against f for their experiments. Their data show some scatter but it is much better fitted by $u_1 \propto f$ than by $u_1 \propto f^{\frac{3}{4}}$. The results of §4 also demonstrate that the small density difference across the mixed layer does not significantly affect the velocity scale u_1.

Most of the experiments on entrainment with zero mean shear have been done with liquids in tanks the same size as Turner's, but Hopfinger & Toly (1976) used a bigger tank with different grids and strokes of oscillation. Their Reynolds number was in the range $230 \leqslant u_1 l/\nu \leqslant 700$ (as compared to $15 \leqslant u_1 l/\nu \leqslant 30$ in Turner's experiments). Hopfinger & Toly did some experiments with common salt in which they measured the entrainment velocity u_e and they found that $u_e/u_1 \propto Ri^{-\frac{3}{2}}$ with the same constant

† On the basis of these measurements, Long has recently revised his argument (see Long, 1978).

of proportionality as Turner (1968). This confirms that at high Richardson numbers the entrainment is independent of the Reynolds number. Hopfinger & Toly also investigated the influence of the mesh size and the stroke of the oscillations on the turbulent velocity field, and they suggest the following formula for the root-mean-square horizontal velocity u_1 at a distance z from the mean position of the grid,

$$\frac{u_1}{fS} = 0{\cdot}25 S^{\frac{1}{2}} M^{\frac{1}{2}} z^{-1}, \tag{4}$$

where S is the stroke of grid oscillations and M is the mesh size of the grid (i.e. the distance between bar centre-lines). Both of the grids they used had the width of each bar equal to one-fifth of M and this is the same ratio that is used in the present investigation.

The degree to which such a mixing box produces spatially homogeneous turbulence is investigated in § 3 of this paper by taking velocity measurements at fixed points in the horizontal plane two grid mesh distances from the grid. Surprisingly large horizontal variations of the turbulence are found. Section 4 addresses the important question of the influence of the very small density gradient in the mixed layer on the turbulence therein, and some measurements are also presented of the turbulence through a density interface.

2. Equipment and instrumentation

2.1. *Equipment*

The experiments of this paper were conducted in a mixing box which was essentially the same as that used by Turner (1968) and described by him in that paper. The only significant improvement was that the grid was oscillated by a speed-controlled d.c. motor and its oscillation frequency was continuously adjustable in the range from 1 Hz to 10 Hz.

2.2. *Laser-Doppler anemometer*

The laser-Doppler anemometer was built by the author at the Department of Applied Mathematics and Theoretical Physics at the University of Cambridge and it is of the digital counter type. It measures the time of flight of small particles across a predetermined number (8 or 16) of fringes in the probe volume. Because of the small (almost zero) mean velocities in the mixing box, it is necessary to have a frequency shift between the two laser beams, and this is accomplished by a rotating, radial diffraction grating. This grating has 10800 chromium-ruled, radial lines around the edge of a glass disc. This disc is attached to a shaft and large brass flywheel which rotate in precision ball bearings. The flywheel is driven by a speed-controlled d.c. motor through a rubber (turntable) belt which passes around the outer circumference of the flywheel. The frequency shift can be varied from 1·5 kHz to 22 kHz with a relative accuracy of better than 1% over the whole range and better than $\frac{1}{3}$% over most of this range. To change the direction of velocity measurement (from say horizontal to vertical) the whole assembly (grating, flywheel, shaft and bearing housings) is rotated about an axis which is made to coincide with the laser beam. This is achieved by shining the laser beam through the centre of a hollow nut which is the pivot axis for the diffraction grating assembly. This assembly was designed in association with Dr Chris Abell.

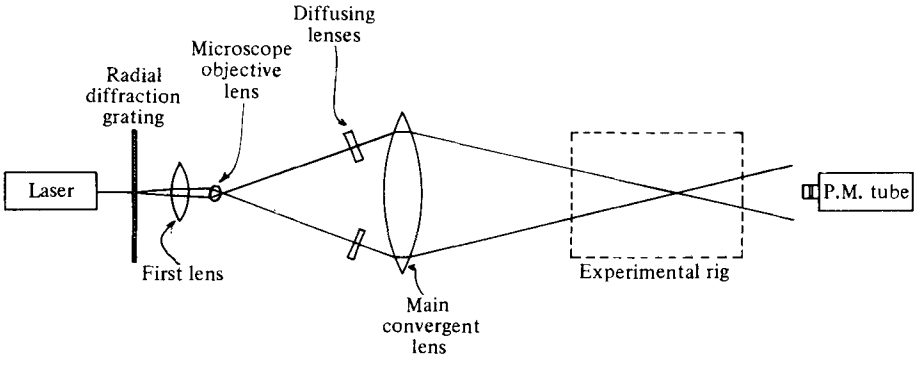

FIGURE 1. Sketch of the laser-Doppler anemometer, set up in the 'fringe' mode.

Figure 1 shows a sketch of the paths of the two laser beams. Note especially the two 'diffusing lenses'. These are very weak divergent lenses (1000 mm focal length) and they were used to obtain a large probe volume. They have the effect of moving the minimum laser beam diameter (i.e. the beam waist) past the probe volume. It was found in practice that any errors due to uneven fringe spacing were negligible. The diameter of the probe volume in the experiments was approximately 300 μm and the fringe spacing was 5·395 μm. Detailed information on the optics and an outline of the design of the digital electronics can be found in McDougall (1978).

2.3. *Method of avoiding refractive index variations*

The variations of refractive index in stratified liquid flows have been a major impediment to the use of laser-Doppler anemometry in these situations. We have developed a method whereby these refractive index variations can be drastically reduced while retaining the dynamically important density differences.

The method uses two different solutes to obtain solutions with the same refractive index but different densities. These solutions are then used to produce the stratified flow. There is however an extra hurdle to overcome, and this is the phenomenon of double diffusive convection which, if present, would cause unwanted fluid motions. Huppert & Manins (1973) have derived a limiting condition for the formation of salt fingers at a density interface and by using their result it is possible to find a pair of solutes which do not give rise to double diffusive convection. A suitable pair of solutes was found to be cane sugar and Epsom salts ($MgSO_4$).

It is usually impossible to use a laser-Doppler anemometer (LDA) in a normal stratified liquid flow because of the large movement of the laser beams which is caused by the refractive index variations. As an example, if a laser beam is passed through 0·25 m of a typical laboratory turbulent environment in which the maximum relative density difference is 1 % (caused by different concentrations of, say, common salt) then the beams are observed to move laterally by up to 10 mm. For this reason Hopfinger & Toly (1976) found it impossible to use an LDA in a mixed layer which was entraining fluid across a density interface. Experiments are described in this paper in which this method has been used to take velocity measurements in a mixed layer and also through a density interface across which the relative density difference was as high as $1\frac{1}{2}$ % and no extra difficulties were encountered with the LDA due to working with a

stratified fluid. This method of matching refractive indices is described in detail in McDougall (1979*a*).

2.4. *Velocity bias correction for the LDA data*

When the arrival rate of light-scattering particles in the probe volume of an LDA is not high enough to be able to reconstruct the velocity *versus* time trace, all real time information (including autocorrelations and spectra) is lost. The particle arrival rate in the mixing box experiments described in this paper was not usually high enough to enable real time data analysis. The cause of this was the zero mean flow character of the velocity field. This problem could not simply be overcome by increasing the seeding concentration because then the laser light intensity would have been severely attenuated.

Although each individual velocity measurement from an individual realization (i.e. counter type) LDA is free from the many ambiguities which are inherent in other types of LDA, a collection of individual velocity readings can still be difficult to interpret because of the effects of biasing. The biasing problem arises because the number of particles per second which pass through the probe volume depends on *all three* components of the velocity vector, while usually only one velocity component is measured.

McLaughlin & Tiederman (1973) were the first to consider the problem of velocity bias. They dealt with the case of a spherical probe volume and a one-dimensional flow, and they showed that the bias could be removed by weighting each measurement with a weighting function which was proportional to the inverse of the measured velocity component. This simple type of correction is inadequate for most common flow configurations because of three important effects. Firstly, the probe volume is usually an ellipsoid with one axis considerably larger than the other two axes, secondly, the flow is seldom one-dimensional and, thirdly, not all particles which pass through the probe volume produce a velocity measurement. This last effect is due to the electronic requirement that a particle must cross a certain number of fringes inside the probe volume, in order for a measurement to be made. These three effects have been studied by Dimotakis (1976) who describes a method of removing the velocity bias for an LDA which simultaneously measures two perpendicular velocity components of a particle. Hoesel & Rodi (1977) have shown how the velocity bias may be easily removed from the data of an LDA which measures (i) one velocity component and (ii) the time which each particle spends inside the probe volume (particle residence time). We have developed a method which applies to the more usual (or older) type of individual realization LDA which measures one velocity component only. This method is summarized below, but is explained in detail in McDougall (1979*b*).

The expected number of measurements per second (i.e. the data rate) is derived for an ellipsoidal probe volume. This expected data rate is a function of the three velocity components of the flow. It is shown that provided the probe volume is not too small (or, equivalently, that the number of Doppler cycles required to yield a measurement is not too large) then almost every particle which enters the probe volume produces a measurement. The addition of a frequency shift between the two laser beams strengthens this approximation.

This expected data rate is used together with an assumed three-dimensional Gaussian turbulence field to form a theoretical biased velocity probability density function, as a function of four parameters. Estimates of two of these parameters

have to be supplied and then the best fit between the theoretical and the experimental biased p.d.f.s gives the values of the mean velocity and the root-mean-square velocity of the flow.

The method needs estimates of (i) the mean velocity in the direction normal to the plane of the laser beams, and (ii) of the ratio of the r.m.s. velocity in the direction of measurement to that in the direction normal to the plane of the laser beams. The method is shown to be quite insensitive to (ii) and only a reasonable estimate of (i) is required. Skewness in the velocity field is also investigated, and it is shown that this does not influence the results very strongly.

This method of overcoming the velocity bias enabled the root mean square and the mean velocities to be determined with a relative accuracy of $\pm 5\frac{1}{2}\%$ (this being the standard deviation of the measurement errors).

2.5. *Method of seeding the flow*

Various types of seeding particles were added to the water to act as scatterers for the laser light. These included milk, tea, liquid toothpaste, titanium dioxide and aluminium oxide, but by far the most successful additive was lycopodium. This was normally used at a concentration sufficient to obtain a suitable particle in the probe volume for about one tenth of the time. A heaped teaspoon of the commercially available lycopodium was first mixed in about a litre of hot water (with the aid of a little detergent) and then this was carefully poured on top of four litres of water (at room temperature) in a large beaker. The larger lycopodium particles then fell slowly through the colder water, leaving the smaller particles behind in the upper region of the beaker. After about half an hour, the water near the bottom of the beaker (containing the larger particles) was siphoned off and this was diluted and used to seed the water in the tank. The lycopodium particles that were obtained in this way were estimated to have diameters of approximately 10 μm.

3. Velocity measurements in a homogeneous fluid

Previous investigators (Thompson & Turner 1975; Hopfinger & Toly 1976) have measured the velocity field with a homogeneous fluid in a mixing box. Thompson & Turner used a hot-film probe which they rotated one revolution at a time in the horizontal plane. Hopfinger & Toly's measurements were mainly made with a continuously rotating hot-film probe or X-probe, although some of their measurements were made with a laser-Doppler anemometer. Thompson & Turner measured only the horizontal velocity component, whereas Hopfinger & Toly measured both the horizontal and the vertical components. In this section we present horizontal and vertical velocity measurements which were made at fixed positions in the mixing box. The previous experimental work yielded spatially averaged velocities but here we investigate the amount of non-uniformity that exists in the horizontal plane.

Two different Perspex grids were used to produce the turbulence in the experiments. Both had a spacing of 50 mm between bars and the bars were 10×10 mm square in cross-section. In all the experiments of this paper, the grids were oscillated with a stroke (i.e. double the amplitude) of 10 mm. One grid was fixed to the central $\frac{1}{4}$ in. stainless-steel rod by a rigid screwed connexion and the other grid had a clip arrange-

	Mean upwards velocity (mm s^{-1})	R.m.s. vertical velocity (mm s^{-1})
Seeding poured into tank above point *o*	+0·33	4·26
Grid oscillations started from rest	+1·50	3·59
Seeding poured into tank above point *d*	+2·58	5·37

TABLE 1. Vertical velocities at position *t* (see figure 2) in the tank, 100 mm above the rigid grid which was oscillated at 5 Hz. The measurements were made between 30 minutes and 60 minutes after the grid oscillations were begun.

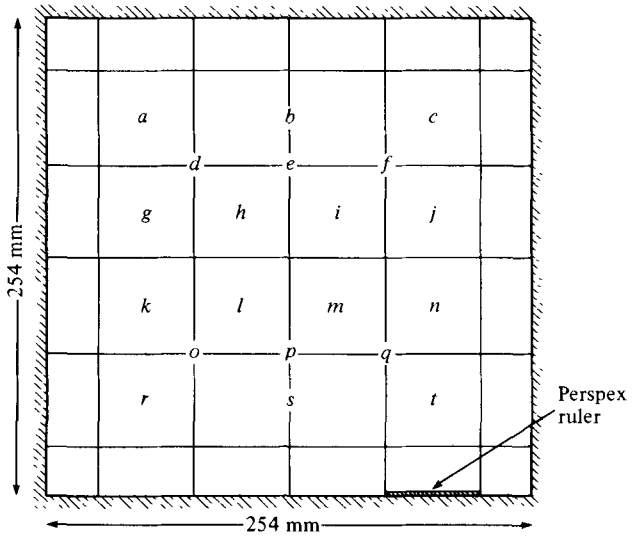

FIGURE 2. Plan view of tank; the positions of measurements in table 2 are indicated by letters. The Perspex rule fits neatly between two of the bars of the grid and is used to guide the grid (see Turner, 1968).

ment which gripped the rod with the force of a metal spring. It proved to be very convenient to be able to adjust the height of this grid without using a screwdriver. This adjustable grid gripped the central rod firmly in that the grid could not move up or down the rod, but, in contrast to the fixed grid, it could wobble vertically about the centre as pivot. This slackness was such that the edge of the grid could move freely by ± 1 mm relative to the centre.

In some of the early experiments (which are not reported here) the tank was first filled with water, the grid was set oscillating, and then the seeding was introduced by pouring about 500 ml of a concentrated water-seeding mixture from a beaker into the tank. This started a large-scale mean circulating motion in the tank which became a permanent feature of the flow. Table 1 gives values of the vertical velocity taken at position *t* (see also figure 2) in the tank when the seeding had been poured onto different areas of the water surface.

Position (see figure 2)	Rigidly attached grid		Adjustable grid	
	Mean	r.m.s.	Mean	r.m.s.
a	+0·60	2·92	−0·13	1·86
b	−0·52	3·06	+0·20	3·05
c	+0·50	3·15	−0·58	3·31
d	−0·97	3·34	−2·37	3·31
e	−2·52	3·38	−1·01	2·80
f	−2·16	3·22	−1·73	3·13
g	+0·78	2·07	+0·27	3·57
h	−1·00	2·59	−2·73	3·23
i	−3·83	2·77	−1·71	3·04
j	+0·27	3·24	−1·35	4·21
k	+1·00	2·74	+1·01	3·03
l	+1·77	3·11	+0·85	2·95
m	−1·42	2·80	−1·04	2·86
n	+0·85	3·20	+0·45	2·92
o	+2·20	3·44	+1·05	2·66
p	−0·69	2·35	+0·08	1·88
q	+1·02	2·57	+1·52	2·77
r	+0·34	1·37	−0·31	2·30
s	−0·50	1·82	−0·53	2·90
t	+1·39	3·18	+1·50	3·59

TABLE 2. Mean and r.m.s. horizontal velocities in the plane 100 mm above the oscillating grid. The grid oscillation frequency was 5 Hz and the stroke was 10 mm. All the entries are in mm s^{-1}.

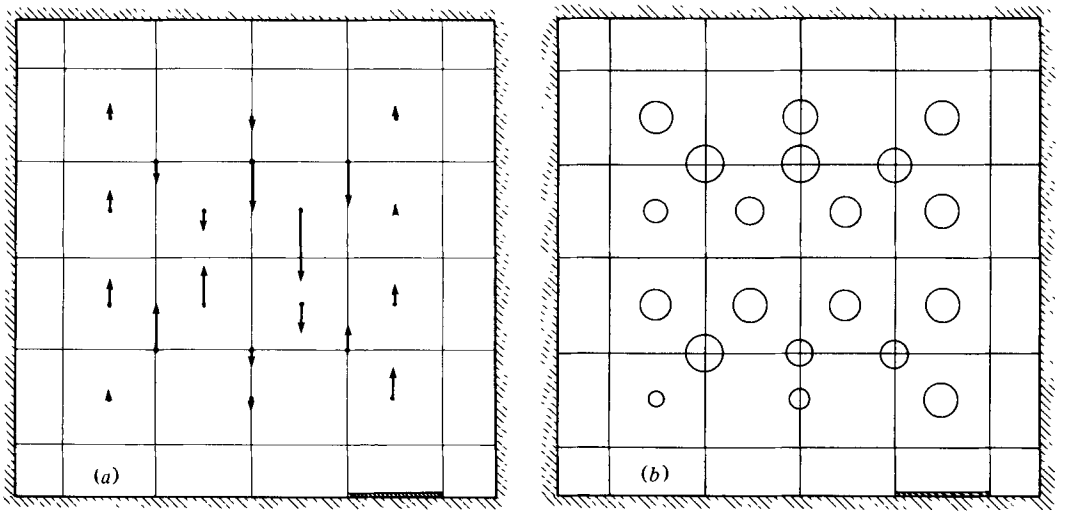

FIGURE 3. (*a*) Mean and (*b*) root-mean-square horizontal velocities in the plane 100 mm from the *rigid* grid. The length and direction of the arrows in (*a*) indicate the mean velocity at each point in the direction shown. The diameters of the circles in (*b*) are proportional to the r.m.s. velocity at each point. The grid was oscillated at a frequency of 5 Hz and a stroke of 10 mm.

This and other similar data showed that, with the grid oscillating, any mean motion which was imparted to the fluid persisted for surprisingly long times. If the grid was not oscillating, this same mean flow died away within a few minutes. An important mean

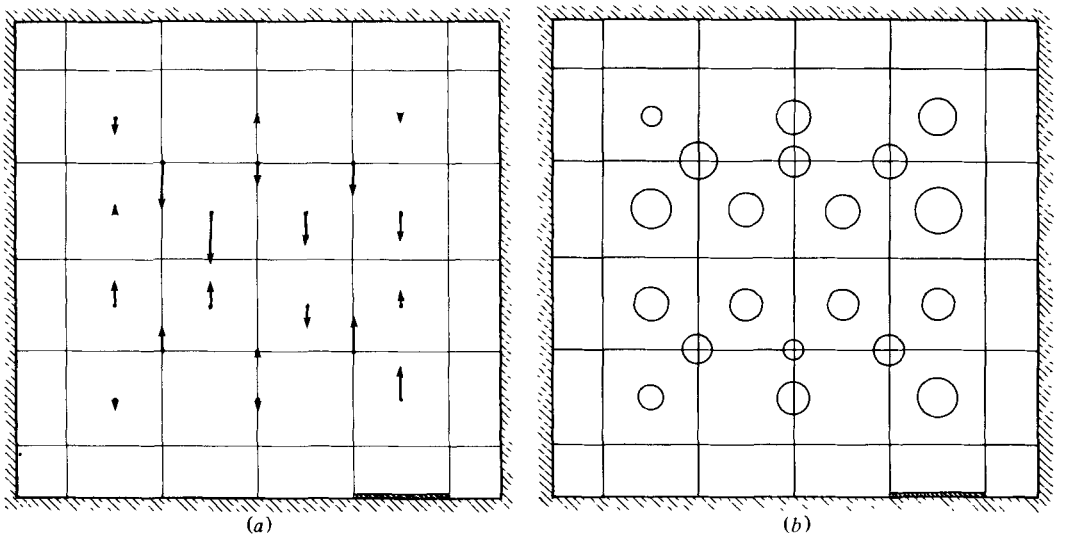

FIGURE 4. (*a*) Mean and (*b*) root-mean-square horizontal velocities in the plane 100 mm from the *adjustable* grid. The length and direction of the arrows in (*a*) indicate the mean velocity at each point in the direction shown. The diameters of the circles in (*b*) are proportional to the r.m.s. velocity at each point. The grid was oscillated at a frequency of 5 Hz and a stroke of 10 mm.

circulating flow also occurred when the grid was oscillated at a high frequency and this is discussed below. For all the other measurements reported in this paper, the seeding was mixed with the fluid before the tank was filled, and the grid oscillations were begun when there was no noticeable fluid movement in the tank. Measurements at fixed positions in the tank were then found to be reproducible from hour to hour and from day to day. This was perhaps surprising (and fortunate) in view of the observed persistence of deliberately imposed mean motions.

3.1. *Velocity measurements 100 mm from the grid*

Table 2 gives the mean and the root-mean-square horizontal velocities at various positions in the horizontal plane 100 mm above the mean position of the grid (see figure 2). Data is shown in this table for both grids (only one grid was used in any particular experiment) and all the measurements were taken at a grid oscillation frequency of 5Hz. These results are shown more clearly in figures 3 and 4. Approximately half of these measurements are the result of two or more readings; often taken on different days, and the agreement between these readings was consistent with the $5\frac{1}{2}$% error bars. The most striking feature of this data is the large variation of the r.m.s. velocity between different positions in the horizontal plane. The smallest value for the fixed grid is 1·37 mm s^{-1} and the largest is 3·44 mm s^{-1}. There is no consistent trend for the velocities to be higher (or lower) over the bar intersection points. There are some similarities in the patterns of high and low r.m.s. velocities for the two grids, but the differences between the grids are quite marked at positions *a*, *g*, *j*, *o* and *s* (see figure 2). The mean horizontal velocities show no obvious patterns and there are again some marked differences between the two grids.

Position (see figure 5)	Mean upwards velocity (mm s^{-1})	R.m.s. vertical velocity (mm s^{-1})
1	+3·72	4·63
2	+2·68	5·86
3	+6·05	4·82
4	−1·60	2·40
5	+0·63	2·73
6	−1·13	2·79
7	+1·52	4·89

TABLE 3. Mean and r.m.s. vertical velocities in the horizontal plane 100 mm above the rigid grid. The grid oscillation frequency was 5 Hz and the stroke was 10 mm.

These results show that the detailed distribution of turbulent kinetic energy and the patterns of mean flow are both quite sensitive to the detailed physical characteristics of the oscillating grid. It is to be hoped that the average kinetic energy over a horizontal plane is not as sensitive to the details of the grid.

The average of the twenty values of the r.m.s. horizontal velocity presented in table 2 is 2·84 mm s^{-1} for the rigid grid and 2·97 mm s^{-1} for the adjustable grid. While these averages are not the true spatial averages (because of there being only 20 values, and these not being equally spaced in the plane) it is clear that there is not a large difference between them in spite of the rather different patterns of r.m.s. velocities shown in figures 3(*b*) and 4(*b*).

Thompson (1969) took measurements of the spatially averaged r.m.s. horizontal velocity in a mixing box the same size as the present one and with the same (fixed) grid. For an oscillating frequency of 5 Hz and a stroke of 10 mm, he obtained an r.m.s velocity of 2·25 ± 0·2 mm s^{-1} at 100 mm from the grid (see Thompson's figure 5.3). It should be noted that the two sets of measurements are very different. Our measurements were taken at fixed positions in the tank whereas Thompson's results were obtained from a series of spatial traverses around a circular path. Thompson & Turner (1975) noted that the mean of each circular traverse (or 'record') was displaced from the true mean 'with a variance that was a significant fraction of the variance of the record'. In his data analysis, Thompson subtracted the mean of *each record* from all the data of that record, *before* any other calculations. This was necessary to be able to calculate spectra. He attempted to compensate for this operation (see the appendix of Thompson & Turner, 1975), but it would seem that this is the main reason for the large discrepancy between our measurements and his (2·84 mm s^{-1} as opposed to 2·25 mm s^{-1}; i.e. our measurements are 26% higher than Thompson's). Hopfinger & Toly (1976) also found this discrepancy and they noted that the formula which they gave for the r.m.s. velocity [their equation (4)] underestimated their data by 20% and overestimated the data of Thompson & Turner by 20%. We note that the Reynolds number was very different in these two sets of experiments. In our experiments the turbulence Reynolds number $u_1 l/\nu$ was about 40, while in Hopfinger & Toly's experiments it was several hundred.

Table 3 gives the mean and r.m.s. *vertical* velocities at a few positions in the horizontal plane 100 mm above the rigid grid (see figure 5). The r.m.s. vertical velocities are

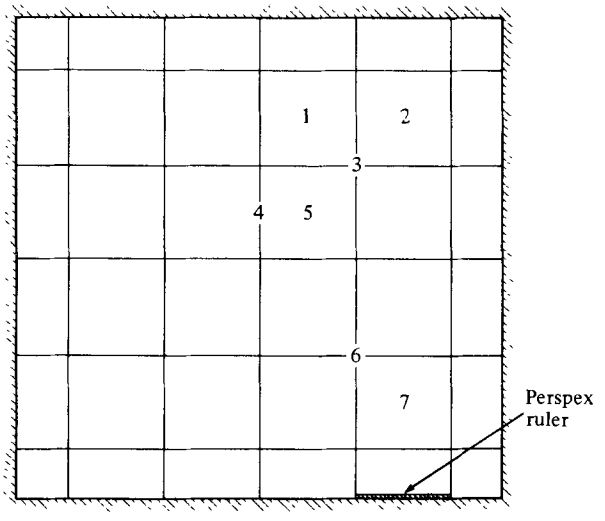

FIGURE 5. Plan view of tank; the positions of measurements in table 3 are indicated by numbers.

larger (40 % larger on average) then the corresponding r.m.s. horizontal velocities (for those measurement positions which coincide), but no further systematic study was made of the spatial variation of the vertical velocities.

3.2. *Dependence of the r.m.s. horizontal velocity on the grid oscillation frequency*

The horizontal velocity was measured at three separate positions in the tank for a range of grid oscillation frequencies. Figure 6 is a plot of the r.m.s. horizontal velocity (u_1) at position f (see figure 2), 100 mm above the rigid grid. This shows that the r.m.s. horizontal velocity is proportional to the grid oscillation frequency up to 7 Hz, but not for frequencies higher than this. Thompson (1969) and Hopfinger & Toly (1976) both found this proportionality, but the maximum grid oscillation frequency used in both of these studies was 6 Hz. This anomalous behaviour at large f was also evident in the horizontal velocities at two other positions in the tank. In order to discover what was causing this behaviour, fine aluminium particles were added to the water and a 10 mm-wide vertical slit of the tank was illuminated by a projector. This vertical slit of light was along the line *o–d* (see figure 2). Figure 7 (plate 1) shows two streak photographs of these aluminium particles: figure 7 (*a*) with the grid oscillating at 4·5 Hz and figure 7 (*b*) at 9·0 Hz. The velocity field looks quite random at 4·5 Hz, but a large mean circulation is evident at 9·0 Hz. It proved to be difficult to obtain streak photographs of the fast motions near the grid. No steady streaming flows were seen emerging from the intersections of the bars, and this is in keeping with the observations of Thompson & Turner (1975, p. 352) for this grid of square bars. However, visual observations indicated that fluid was *intermittently* shed *vertically* from the grid intersection points when the grid was oscillated at 4·5 Hz, but at 9 Hz the fluid was shed in more random directions. The exposure times of the two photographs (figures 7 (*a*), (*b*)) are different, and so the lengths of the streaks cannot be directly compared, but it is evident that at 9 Hz the mean circulation (up the right-hand side of the photograph and down the left-hand side) completely dominated the flow. The turbulence from the grid on the

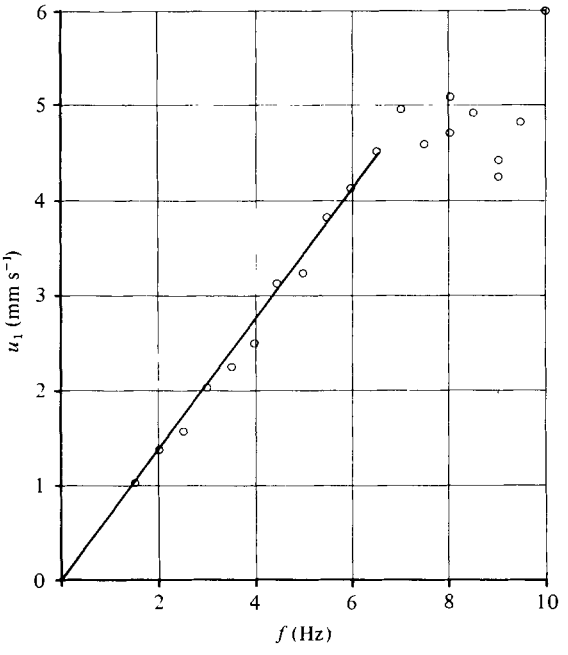

FIGURE 6. Values of the r.m.s. horizontal velocity u_1 as a function of the grid oscillation frequency f at a fixed position in the tank. This position is 100 mm above the grid at point f (see figure 2).

left-hand side only reached 80 mm from the grid before it was opposed by the downcoming mean flow. In figure 7 the rigid grid was used, but a similar mean circulating flow was observed with the adjustable grid at these high oscillation frequencies. The cause of this behaviour is unknown but, when the grid was oscillated at a stroke of 20 mm, the mean circulating flow still appeared. It is not known for instance if this behaviour would have occurred in Hopfinger & Toly's tank if higher oscillation frequencies had been used. Because of this unwanted circulating motion at high grid oscillation frequencies, the maximum frequency which was used in the rest of the experiments was 6 Hz.

4. Velocity measurements in the presence of a density interface

4.1. *Stability of the steady-state, mid-depth density interface*

In some of the experiments of this section, a steady-state density interface was set up between two well-mixed layers by using the method of Thompson (1969, p. 122). Two fluid layers of equal depth were placed in the tank, one above the other; fluid of density ρ_1 underlying fluid of density ρ_2. A grid of bars was located in the middle of each layer, and these grids were oscillated at the same frequency and stroke (the oscillations were also in phase). In order to maintain a steady-state, equal volume flow rates of fluid of density ρ_{1R} ($\rho_{1R} > \rho_1$) and of fluid of density ρ_{2R} ($\rho_{2R} < \rho_2$), were fed into the lower and the upper layers respectively. Double this volume flow rate was withdrawn from the interfacial region through four holes in the sides of the tank. These flow rates were metered and they were driven by constant-head supply tanks.

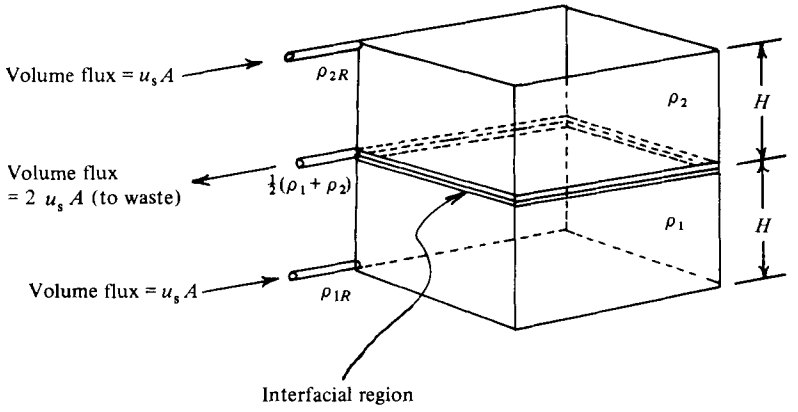

FIGURE 8. Sketch of the mixing box with two well-mixed layers (both of depth H) in a steady-state situation. H was 215 mm in all experiments.

The steady-state density difference $(\rho_1-\rho_2)$ between the two well-mixed layers is determined by the supply volume flow rates of the reservoir fluids, the density difference $\rho_{1R}-\rho_{2R}$ between the reservoir solutions, and the characteristics of the oscillating grids. In this steady state, the entrainment of buoyancy across the density interface into each well-mixed layer is in balance with the external supply of buoyancy from the reservoirs. The entrainment across the density interface is in turn dependent on $\rho_1-\rho_2$ and, because of this, it is not possible in some cases to establish a steady-state situation with a low value of the ratio $(\rho_1-\rho_2)/(\rho_{1R}-\rho_{2R})$, even though the expected buoyancy fluxes (due to entrainment and supply from the reservoirs) would be equal. In this case the steady state is unstable and, if an attempt is made to establish it, the density difference between the layers will either disappear (i.e. $\rho_1=\rho_2$) or it will increase to a larger stable value. This instability is investigated here.

Figure 8 shows the two well-mixed layers in the mixing box. We define the supply velocity u_s to be the volume supply rate of fluid to the top or bottom layer, divided by the horizontal area A of the tank. u_s was always much less than the typical turbulent velocity in the mixed layer: at most u_s was 1 % of u_1. Conservation of mass in layers 1 and 2 gives

$$\frac{d}{dt}(H\rho_1) = -u_e(\rho_1-\rho_2)+u_s(\rho_{1R}-\rho_1), \tag{5}$$

and

$$\frac{d}{dt}(H\rho_2) = u_e(\rho_1-\rho_2)-u_s(\rho_2-\rho_{2R}), \tag{6}$$

where H is the depth of both of the layers and u_e is the entrainment velocity [i.e. the entrainment flux of buoyancy divided by $gA(\rho_1-\rho_2)$] across the density interface. u_e is assumed to be the same for the entrainment into both of the layers. Subtracting (6) from (5), we obtain

$$\frac{d}{dt}(\rho_1-\rho_2)+\frac{u_s+2u_e}{H}(\rho_1-\rho_2) = \frac{u_s}{H}(\rho_{1R}-\rho_{2R}). \tag{7}$$

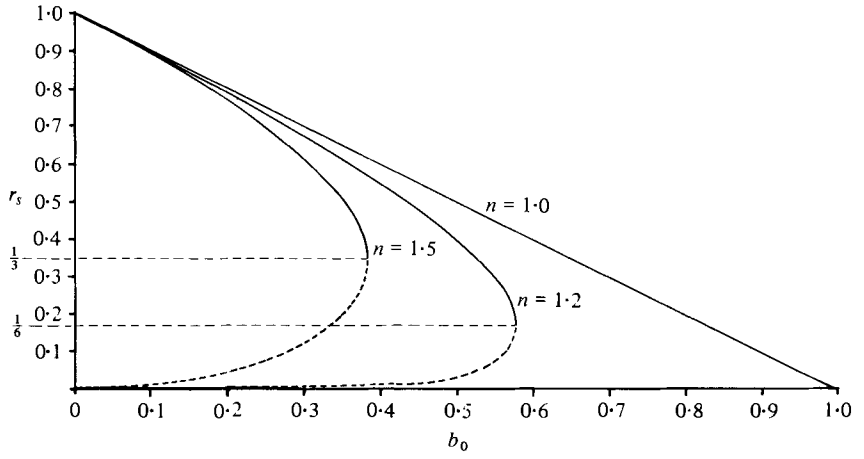

FIGURE 9. Plots of the steady-state value of $(\rho_1-\rho_2)/(\rho_{1R}-\rho_{2R})$ (i.e. r_s) against b_0 for three values of n. These plots are simply the solutions of equation (11). The upper branches (full lines) are stable and the lower branches (dashed lines) are unstable.

When the system has reached a steady state, we see from this equation that the final value of $\rho_1-\rho_2$ is given by

$$\frac{\rho_1-\rho_2}{\rho_{1R}-\rho_{2R}} = \frac{u_s}{u_s+2u_e}. \tag{8}$$

The entrainment velocity u_e is usually expressed as

$$\frac{u_e}{u_1} = c_0\left[\frac{g(\rho_1-\rho_2)\,l}{\rho_r u_1^2}\right]^{-n} \tag{9}$$

where u_1 is the velocity scale and l is the length scale of the turbulence near the interface; ρ_r is a reference density. Putting $(\rho_1-\rho_2)/(\rho_{1R}-\rho_{2R}) = r$ and using (9), (7) becomes

$$\frac{H}{u_s}\frac{dr}{dt} - (1-r) + b_0 r^{1-n} = 0; \quad \text{where} \quad b_0 = \frac{2u_1}{u_s}c_0\left[\frac{g(\rho_{1R}-\rho_{2R})}{\rho_r u_1^2}l\right]^{-n}. \tag{10}$$

Let r_s be a solution of the steady-state situation, that is

$$-(1-r_s) + b_0 r_s^{1-n} = 0. \tag{11}$$

We examine the stability of this solution by putting $r = r_s+\epsilon$ ($\epsilon \ll r_s$) in (10) and retaining terms to first order in ϵ. This gives

$$\frac{1}{\epsilon}\frac{d\epsilon}{dt} = -\frac{u_s}{Hr_s}(1-n(1-r_s)), \tag{12}$$

and the right-hand side of this equation must be negative if infinitesimal disturbances to the steady solution are to decay. This requires $r_s > (n-1)/n$. The value of the exponent n depends on the stratifying agent and commonly quoted values of n are 1·0 for heat and 1·5 for common salt. In the entrainment experiments of this paper, both of the mixed layers are a mixture of an Epsom-salts solution and a sugar solution.

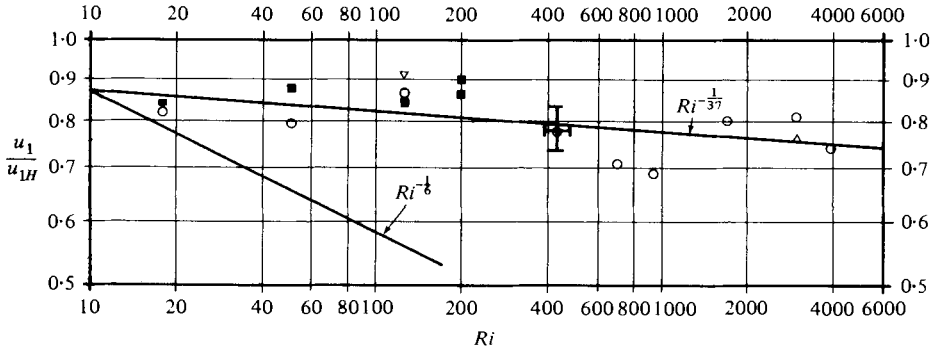

FIGURE 10. Graph of the r.m.s. horizontal velocity (u_1) 22·5 mm below the centre of a density interface, divided by the corresponding velocity measured in a deep homogeneous layer of fluid at the same position (u_{1H}). The abscissa is the interfacial Richardson number $g(\rho_1-\rho_2)\,l/\rho_0\,u_1^2$. Grid oscillation frequencies of 2, 3, 4, 5 and 6 Hz were used for these measurements. ■, position f in tank, steady-state system; ○, position f in tank, quasi-steady; ▽, position q in tank, steady-state system; △, position q in tank, quasi-steady.

The values of n for both of these solutes are close to 1·5. Figure 9 shows graphs of r_s against b_0 for three different values of n; these graphs being plotted from (11). The important point of this figure is not the numerical values of b_0, but rather that, for any given value of b_0, there are two solutions for r_s (for $n > 1$), the larger of which is stable and the smaller of which is unstable.

In all the experiments in which this steady-state apparatus was used, the value of r_s was chosen to be close to 0·5 and so this ensured that a stable steady state was reached. In practice, l was kept constant and the interfacial Richardson number $(g(\rho_1-\rho_2)\,l/\rho_r u_1^2)$ then depended only on $(\rho_1-\rho_2)$ and u_1. Choosing a grid oscillation frequency (this determining u_1) and a desired Richardson number, gave the required density difference $\rho_1-\rho_2$. The chosen value of r_s (= 0·5) then set $\rho_{1R}-\rho_{2R}$. The entrainment velocity u_e was then read from Turner's data (Turner 1973, figure 9.3), and the supply velocity u_s was set equal to $2u_e$ [see (8)]. In each of the experiments then, ρ_{1R}, ρ_{2R} and u_s were held fixed, and ρ_1 and ρ_2 were initially set equal to the values which were calculated by the above procedure. We do not expect to be able to set u_s to exactly the correct value to obtain the desired steady-state $\rho_1-\rho_2$. One reason for this is that Turner's entrainment data was for common salt and we used a mixture of sugar and Epsom salts in each layer. In any case, the entrainment velocity u_e should be almost the same for both layers because the molecular diffusivities of sugar and Epsom salts in water are similar. Any mismatch between the initial value of $\rho_1-\rho_2$ and the final, steady-state value is expected to disappear with an e-folding time of [from (12)]

$$\tau = \frac{H}{u_s}\frac{r_s}{[1-n(1-r_s)]} \approx \frac{H}{u_s}\frac{1}{(2-n)}.$$

This e-folding time took values between ten minutes and several hours in the experiments.

4.2. *Velocity measurements near a density interface*

In these experiments, the centre of the density interface was 122·5 mm from both grids and the horizontal velocity u_1 was measured 100 mm above the lower grid, that is,

22·5 mm below the centre of the interface. The lower grid was the fixed one and the upper grid was the adjustable one. Measurements were made mostly at one position in this horizontal plane (position *f* of the figure 2) but two measurements were made at another position (position *q*). Some measurements were made with the mixed-layer system in a steady state (see §4.1) and some with the system only quasi-steady; that is, with the density difference $\rho_1 - \rho_2$ slowly decreasing due to entrainment. These quasi-steady experiments still had two well-mixed layers, agitated by a grid in each layer, but there was no supply of fluid from reservoirs and no withdrawal of fluid from the interfacial region. The measurements are shown on log–log axes in figure 10. The ordinate is the r.m.s. horizontal velocity measured 100 mm above the bottom grid u_1 divided by the r.m.s. horizontal velocity measured at exactly the same position in a deep homogeneous layer u_{1H}. The line of best fit has a slope given by $Ri^{-\frac{1}{37}}$ and this is not significantly different to Ri^{-0} (i.e. constant). The $Ri^{-\frac{1}{2}}$ slope is shown for comparison. We note that, in order to test the validity of (3), the abscissa should really be Ri_*, but since it is shown that u_1/u_{1H} is almost constant (i.e. $u_1 \propto f$ and not $u_1 \propto f^{\frac{1}{2}}$), it seems clearer to use the more familiar interfacial Richardson number Ri. The ordinate should similarly be u_1/fS, but S was kept constant during the experiments and u_1/u_{1H} has the added advantage of collapsing the measurements from the two separate positions in the plane.

In the quasi-steady experiments, the rate of working against buoyancy forces in each layer is $\frac{1}{2}gu_e(\rho_1 - \rho_2)H$ per unit horizontal area; this being the flux of excess weight across the density interface per unit area $gu_e(\rho_1 - \rho_2)$ multiplied by the average height $\frac{1}{2}H$ to which this weight is raised or lowered. In the steady-state experiments, additional work against buoyancy forces is required to distribute the reservoir fluid throughout each mixed layer. This amount of power per unit area is $\frac{1}{2}gu_s(\rho_{1R} - \rho_1)H$ for the lower layer and $\frac{1}{2}gu_s(\rho_2 - \rho_{2R})H$ for the upper layer. For a steady state, (5) and (6) give

$$u_s(\rho_{1R} - \rho_1) = u_s(\rho_2 - \rho_{2R}) = u_e(\rho_1 - \rho_2)$$

and so we see that the power required to redistribute the reservoir fluid throughout each mixed layer is equal to that required to redistribute the fluid which is entrained across the density interface. Because of this, the total work done against buoyancy forces in the steady-state experiments is double that in the quasi-steady experiments. Figure 10 shows no obvious differences between the data for the steady and the quasi-steady experiments and this gives further support to the idea that the small density difference across the mixed layer and the associated small rates of working against buoyancy are not dynamically important.

The process by which entrainment occurs must change significantly with the Richardson number (Ri) because at high Ri a significant fraction of the buoyancy flux is due to molecular diffusion down the concentration gradient. If the thickness of the interface is given by h, then the buoyancy flux through the interface which would be achieved by molecular diffusion alone is $g\kappa\Delta\rho/h$, where κ is the molecular diffusivity of the stratifying agent. Taking $h \approx 1{\cdot}5\,l$ (Crapper & Linden 1974) and $l \approx 0{\cdot}1z$ (Thompson & Turner 1975), we have

$$\frac{\text{Total flux}}{\text{Diffusive flux}} = \frac{gu_e\Delta\rho}{g\kappa\Delta\rho/1{\cdot}5l} = 1{\cdot}5\,(0{\cdot}1z)\frac{u_1}{\kappa}\frac{u_e}{u_1}. \tag{13}$$

Now for $f = 5$ Hz, $zu_1 \approx 2{\cdot}2$ cm^2 s^{-1} [see equation (4)] and so (13) becomes

$$\frac{\text{Total flux}}{\text{Diffusive flux}} = 25000\,\frac{u_e}{u_1}. \tag{14}$$

The diffusive flux will be as much as one tenth of the total flux when $u_e/u_1 = 4 \times 10^{-4}$ and, from figure 9.3 of Turner (1973), this occurs when $Ri \approx 600$ (for salt). For $Ri \lesssim 600$, the entrainment occurs by the direct interaction of the turbulent eddies with the interfacial region, whereas for $Ri > 600$, progressively more of the buoyancy flux is due to molecular diffusion and not an entrainment process as such. The data of figure 10 cover a large range of Richardson number (from $Ri = 18$ to 4000) and perhaps the trend for u_1/u_{1H} to be lower for values of $Ri \gtrsim 600$ is due in part to this change of entrainment mechanism at high Richardson numbers.

4.3. *Velocity measurements near a solid wall and through a density interface*

Hunt & Graham (1978) have recently given a theory for the effect on free-stream turbulence of a boundary which moves at the speed of the mean flow. This has also been investigated experimentally by Thomas & Hancock (1977). These authors find that there is a boundary region within which fluctuations of the velocity normal to the wall decrease monotonically. This boundary region scales on the integral length scale l of the turbulence in the free stream and is called the 'source boundary layer' because of the distribution of sources which are needed at the wall (in the theory) to obtain zero normal velocity fluctuations there. Within a distance of approximately $0{\cdot}2l$ from the wall, the fluctuating transverse velocity components become larger than their free-stream values. This can be imagined to be due to the squashing (or flattening) of eddies near the wall. These results apply at large Reynolds numbers and within a downstream distance given by $\bar{U}l/u_1 = \bar{U} \times$ [eddy turn-over time] (where $\bar{U}$ is the mean velocity and u_1 is the free-stream r.m.s. velocity) from some initial origin. The viscous fluctuation boundary-layer thickness must be much less than l in this theory. Figure 11 shows the mean square velocities (for a horizontal moving wall) from Hunt & Graham's theory.

It is not at all clear how this theory might be generalized to zero mean flow turbulence near a wall. It is obvious that the fluctuating velocity component normal to the wall must go to zero at the wall and for high Reynolds numbers we may expect that this component will be significantly affected by the wall within a distance of order l from the wall. Figures 12(*a*), (*b*) show measurements of the horizontal and vertical r.m.s. (and mean square) velocities near a horizontal boundary which was placed in the mixing box 122·5 mm above the oscillating grid of bars. The Reynolds number of the turbulence $u_1 l/\nu$ at 100 mm above the grid was about 40. It can be seen in figure 12(*b*) that the mean square vertical velocity begins to decrease at about one integral length scale l from the boundary (i.e. 10 mm) and this is in agreement with the theory of Hunt & Graham (1978) for the situation with mean flow. The mean square horizontal velocity remains constant right up to 2 mm ($= 0{\cdot}2l$) from the boundary. Even if Hunt & Graham's theory was applicable to this situation, we would not expect any amplification of the horizontal velocity component because of the low Reynolds number of the turbulence.

Figure 13 shows some measurements of the r.m.s. vertical and horizontal velocities

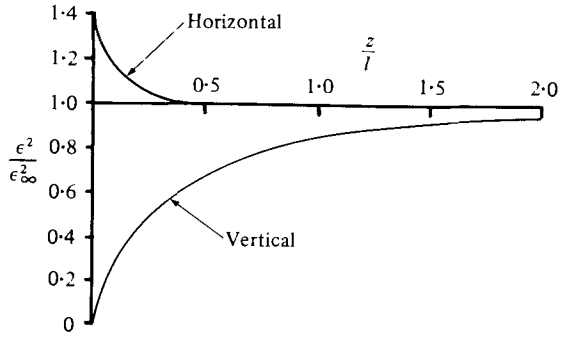

FIGURE 11. Graphs of the mean square ($\mathscr{E}^2$) horizontal and vertical velocities (normalized by the free-stream values ($\mathscr{E}_\infty^2$) of Hunt & Graham's theory. [From figure 5 of Hunt & Graham (1978)].

through three density interfaces. These interfaces were between two well-mixed layers. The $Ri = 26$ interface was in a steady state (as explained in §4.1), and the $Ri = 80$ and $Ri = 280$ interfaces were quasi-steady. The r.m.s. vertical velocities decrease towards the centre of each interface. The r.m.s. vertical velocity at the centre of the interface is smallest for the most stable interface (i.e. $Ri = 280$). The r.m.s. horizontal velocity shows somewhat different behaviour for high and low stability. At $Ri = 26$, the horizontal velocity increases as the interface centre is approached, whereas, at $Ri = 80$ and $Ri = 280$, there is perhaps an initial increase at the edge of the interfacial region and then a definite decrease towards the centre. [The edge of the interfacial region was simply determined by using the Crapper & Linden (1974) result that the thickness of the interfacial region is approximately $1{\cdot}5l$. Shadowgraphs were not of course useful in these three experiments because of the matching of refractive indices.]

The large r.m.s. horizontal velocity and the small r.m.s. vertical velocity in the centre of the low Richardson number interface probably points to the importance of the distortion of the turbulent eddies in a similar manner to the theory of Hunt & Graham. However, the propagation of internal gravity waves almost vertically through the interfacial density gradient region could also account for a large horizontal r.m.s. velocity (A. A. Townsend, personal communication).

There is a hint of some amplification of the horizontal velocity component at $Ri = 80$ and $Ri = 280$ at the edge of the interface while the centre of the interface remains less active. (We do not have enough accurate data to assert this with confidence.) This seems to imply that the turbulent eddies do not often penetrate into the centre of the interface but that they are halted (by the squashing mechanism) near the edge of the interface and visual observations confirm this behaviour.

These results leave many questions unanswered and do not for instance cast any light on the intermittency of the turbulence in the interfacial region, but, now that the problems associated with the refractive index variations can be overcome, we may expect more detailed measurements in the future.

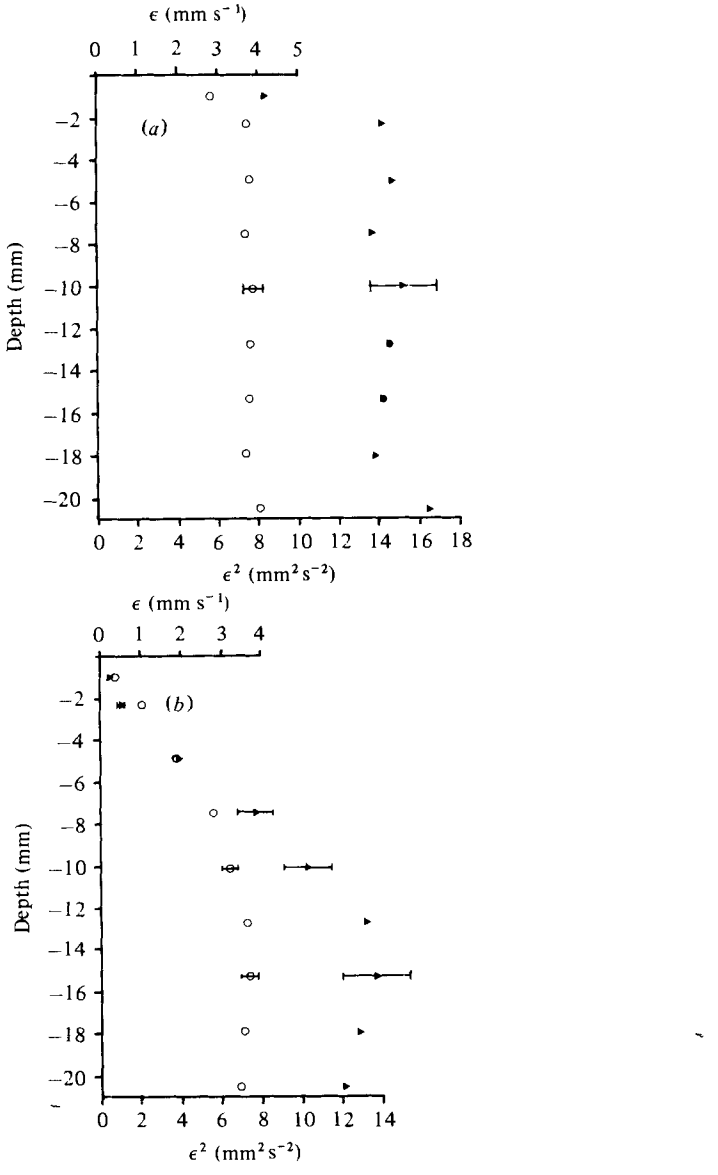

FIGURE 12. Graphs of the r.m.s. ($\mathscr{E}$) and mean square ($\mathscr{E}^2$) (*a*) horizontal and (*b*) vertical velocities at various distances from a solid horizontal boundary at depth = 0 mm. The grid oscillation frequency was 5 Hz and the integral length scale l of the turbulence near the interface was 10 mm.

5. Concluding remarks

Velocity measurements made in a homogeneous fluid 100 mm above an oscillating grid have shown that the velocity field is quite non-uniform and the non-uniformities are not directly correlated with the square pattern of the grid of bars. These non-uniformities do depend however on the exact physical characteristics of the grid

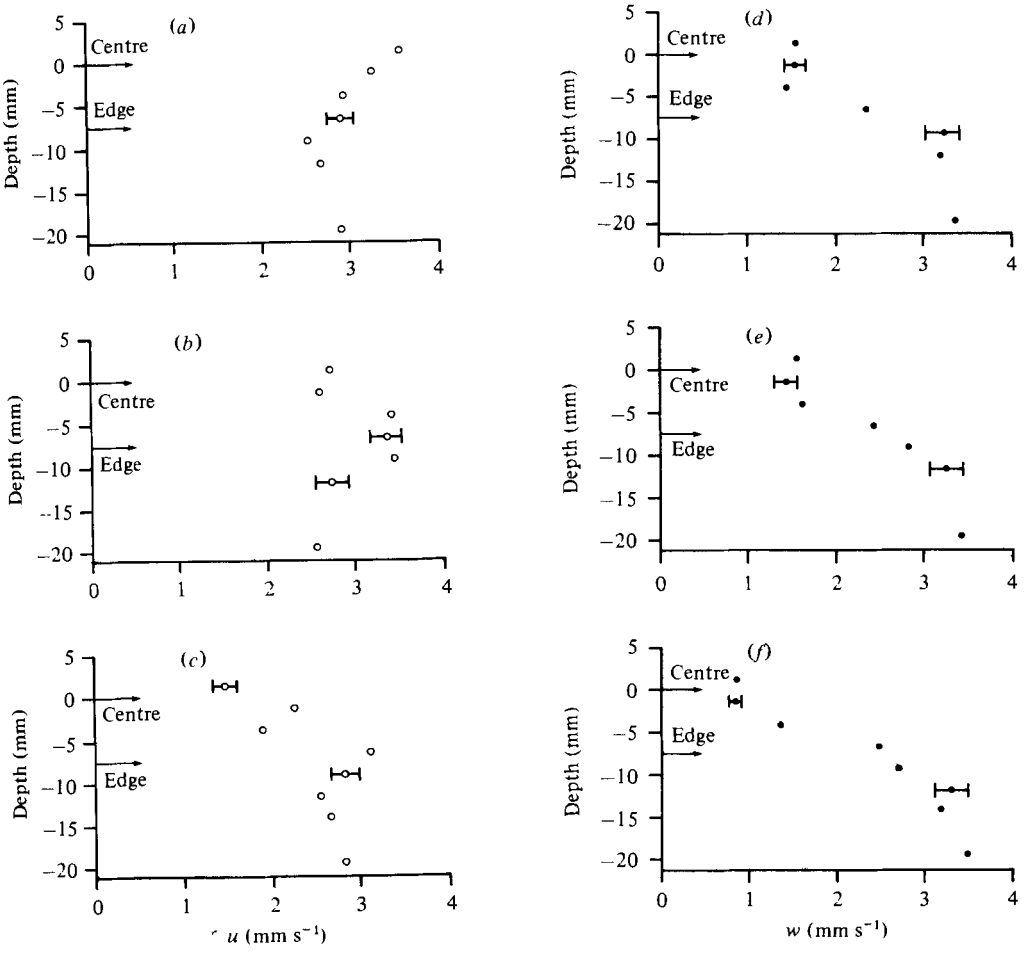

FIGURE 13. Plots of the r.m.s. (*a*, *b*, *c*) horizontal u and (*d*, *e*, *f*) vertical w velocities through three density interfaces. (*a*, *b*) $Ri = 26$; (*b*, *e*) $Ri = 80$; (*c*, *f*) $Ri = 280$. The centre and the edge of the interfacial region are marked by arrows on the ordinate. The grids were oscillated at 5 Hz.

(e.g. its rigidity). The persistence of deliberately imposed mean motions points to the nonlinear character of the formation of a mean flow by an oscillating bar. That is to say, in those regions where the existing mean flow is upwards past part of the grid of bars, the upward part of the grid motion transfers more energy to the flow than does the downgoing part of the oscillation cycle. It is easy then to imagine how small differences in the physical characteristics of the grid can change the detailed patterns of mean and root mean square velocities.

Velocity measurements near the base of a mixed layer have shown that the small density difference across the mixed layer does not significantly effect the turbulence in the mixed layer.

Vertical and horizontal velocity measurements of zero-mean-flow turbulence near a solid wall have shown that the root mean square vertical velocity begins to decrease at about one integral length scale from the wall, whereas the r.m.s. horizontal velocity remains constant right up to one-fifth of an integral length scale from the wall (where

viscosity can directly affect the turbulence). These results bear a striking resemblance to the theory of Hunt & Graham (1978) about the effect of a moving wall on wind-tunnel turbulence, even though this theory is not directly applicable in the absence of a mean flow.

Turbulence measurements through a density interface show that the turbulent eddies appear to be 'squashed' near a density interface in a similar manner to the theory of Hunt & Graham (1978). These measurements have shown some interesting trends with the overall Richardson number of the interface, but much more work remains to be done in this area.

Many helpful discussions with Dr P. F. Linden and Professor J. S. Turner are gratefully acknowledged. The apparatus was ably constructed by Mr Paul Bower-Macer. This work was made possible by a George Murray Overseas Scholarship given by the University of Adelaide and further financial support came from St John's College, Cambridge and the Cambridge Philosophical Society. This work was completed at the Australian National University where I have been supported by a Queen's Fellowship in Marine Science.

REFERENCES

CRAPPER, P. F. & LINDEN, P. F. 1974 The structure of turbulent density interfaces. *J. Fluid Mech.* **65**, 45–63.

DIMOTAKIS, P. E. 1976 Single particle laser Doppler measurements of turbulence. *AGARD Symp. Non-intrusive Instrument. in Fluid Flow Res., Saint-Louis, France*, paper 10.

GILL, A. E. & TURNER, J. S. 1976 A comparison of seasonal thermocline models with observation. *Deep-Sea Res.* **23**, 391–401.

HOESEL, W. & RODI, W. 1977 New biasing elimination method for laser-Doppler velocimeter counter processing. *Rev. Sci. Instrum.* **48**, 910–919.

HOPFINGER, E. J. & TOLY, J.-A. 1976 Spatially decaying turbulence and its relation to mixing across density interfaces. *J. Fluid Mech.* **78**, 155–175.

HUNT, J. C. R. & GRAHAM, J. M. R. 1978 Free-stream turbulence near plane boundaries. *J. Fluid Mech.* **84**, 209–235.

HUPPERT, H. E. & MANINS, P. C. 1973 Limiting conditions for salt-fingering at an interface. *Deep-Sea Res.* **20**, 315–323.

KATO, H. & PHILLIPS, O. M. 1969 On the penetration of a turbulent layer into a stratified fluid. *J. Fluid Mech.* **37**, 643–655.

KRAUS, E. B. & TURNER, J. S. 1967 A one-dimensional model of the seasonal thermocline. II. The general theory and its consequences. *Tellus* **19**, 98–106.

LONG, R. R. 1975 The influence of shear on mixing across density interfaces. *J. Fluid Mech.* **70**, 305–320.

LONG, R. R. 1977 Some aspects of turbulence in geophysical systems. *Adv. Appl. Mech.* **17**, 1–90.

LONG, R. R. 1978 A theory of mixing in a stably stratified fluid. *J. Fluid Mech.* **84**, 113–124.

MCDOUGALL, T. J. 1978 Some aspects of geophysical turbulence. Ph.D. thesis, University of Cambridge.

MCDOUGALL, T. J. 1979*a* On the elimination of refractive index variations in turbulent density-stratified liquid flows. *J. Fluid Mech.* **93**, 83.

MCDOUGALL, T. J. 1979*b* Bias correction for individual realization laser-Doppler anemometer measurements. *J. Phys. E.* (in press).

MCLAUGHLIN, D. K. & TIEDERMAN, W. G. 1973 Biasing correction for individual realization of laser anemometer measurements in turbulent flows. *Phys. Fluids* **16**, 2082–2088.

NIILER, P. P. & KRAUS, E. B. 1977 One-dimensional models. In *Modelling and Prediction of the Upper Layers of the Ocean* (ed. E. B. Kraus). Oxford: Pergamon Press.

THOMAS, N. H. & HANCOCK, P. E. 1977 Grid turbulence near a moving wall. *J. Fluid Mech.* **82**, 481–496.

THOMPSON, S. M. 1969 Turbulent interfaces generated by an oscillating grid in a stably stratified fluid. Ph.D. thesis, University of Cambridge.

THOMPSON, S. M. & TURNER, J. S. 1975 Mixing across an interface due to turbulence generated by an oscillating grid. *J. Fluid Mech.* **67**, 349–368.

TURNER, J. S. 1968 The influence of molecular diffusivity on turbulent entrainment across a density interface. *J. Fluid Mech.* **23**, 639–656.

TURNER, J. S. 1973 *Buoyancy Effects in Fluids.* Cambridge University Press.

TURNER, J. S. & KRAUS, E. B. 1967 A one-dimensional model of the seasonal thermocline. I. A laboratory experiment and its interpretation. *Tellus* **19**, 88–97.

WOLANSKI, E. J. & BRUSH, L. M. 1975 Turbulent entrainment across stable density step structures. *Tellus* **27**, 259–268.

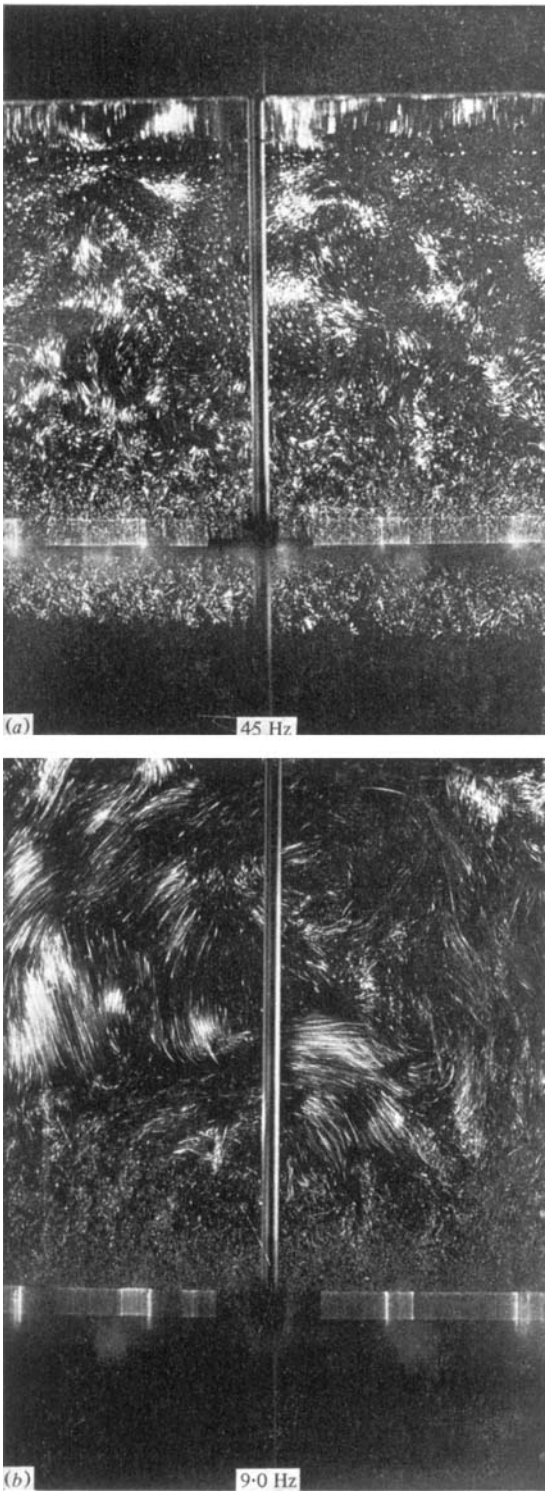

FIGURE 7. Streak photographs of the fluid motion in the tank for a grid oscillation frequency of (*a*) 4·5 Hz and (*b*) 9·0 Hz. The exposure time for figure (*a*) was $\frac{1}{4}$ s and for figure (*b*) was $2\frac{1}{2}$ s.